Available online at www.sciencedirect.com
ScienceDirect
Journal of Sound and Vibration 319 (2009) 77–90
JOURNAL OF SOUND AND VIBRATION
www.elsevier.com/locate/jsvi

Trajectory tracking control of parallel robots in the presence of joint drive flexibility

S. Kemal Ider*, Ozan Korkmaz

Mechanical Engineering Department, Middle East Technical University, Ankara 06531, Turkey

Received 8 September 2007; received in revised form 15 May 2008; accepted 20 May 2008
Handling Editor: M.P. Cartmell
Available online 16 July 2008

Abstract

Trajectory tracking control of parallel manipulators is aimed in the presence of flexibility at the joint drives. Joint structural damping is also considered in the dynamic model. The system is first converted into an open-tree structure by disconnecting a sufficient number of unactuated joints. The closed loops are then expressed by constraint equations. It is shown that, in a parallel robot with flexible joint drives, the acceleration level inverse dynamics equations are singular because the control torques do not have an instantaneous effect on the end-effector accelerations due to the elastic media. Eliminating the Lagrange multipliers and the intermediate variables, a fourth-order input–output relation is obtained between the actuator torques and the end-effector position variables. The proposed control law decouples and linearizes the system and achieves asymptotic stability by feedback of positions and velocities of the actuated joints and rotors. As a case study, a three degree of freedom, two legged planar parallel manipulator is simulated to illustrate the performance of the method. The end-effector desired trajectory is chosen such that the kinematic and drive singular positions are avoided.

1. Introduction

Parallel manipulators have been an intensive area of research for over a decade. Due to their closed-loop structure they can carry heavier loads with greater accuracy compared to serial manipulators. These mechanisms are most commonly used in industrial applications such as flight simulators and earthquake simulators, micro-motion manipulations where high load capability and high motion accuracy are needed. However these manipulators face the problem of having a relatively small functional workspace and difficulties in design and control. For this reason parallel manipulators have become a focus of interest in various fields of research. On the other hand, joint flexibility is important in manipulator dynamics and control system design since their drives exhibit this behavior. Rivin [1] showed experimentally that joint flexibility is the main source contributing to overall robot flexibility, and Good et al. [2] showed empirically that ignoring joint flexibility in controller design of contemporary industrial robots results in performance

*Corresponding author. Tel.: +90 312 210 5239.
E-mail address: kider@metu.edu.tr (S.K. Ider).

0022-460X/$ - see front matter
doi:10.1016/j.jsv.2008.05.025

degradation. Hence in order to handle high precision manipulations, joint flexibility should be taken into consideration in the controller design.

Many researchers studied the control of flexible joint serial manipulators. Spong [3] considered two nonlinear control schemes, namely inverse dynamics and singular perturbation. In the inverse dynamics approach the intermediate variables are analytically eliminated and the input torques are found to be functions of the end-effector motion [3–6]. The singular perturbation approach uses the advantage of order reduction by decomposing the system into two subsystems, namely a fast subsystem (flexible joints) and a slow subsystem (rigid manipulator) [3,7]. Forrest-Barlach and Babcock [4] used the inverse dynamics control method for the cylindrical coordinate arm with drive train compliance and actuator dynamics in the radial and each of the revolute degrees of freedom. Jankowski and Van Brussel [5] applied inverse dynamics control in discrete time where solution of the singular set of differential equations is used to avoid the further differentiations of the system equations of motion. Ider and Özgören [6] utilized inverse dynamics control at the acceleration level by using implicit numerical integration methods that account for the higher order derivative information for solving the singular set of differential equations. They achieved asymptotic stability by the feedback of joint positions, velocities and rotor velocities. Other studies involving control of serial manipulators with flexible joints include simultaneous motion and force control of constrained robots [8–10] and adaptive controllers [11–13]. Recent survey papers by Ozgoli and Taghirad [14], and Dwivedy and Eberhard [15] provide detailed literature reviews of modelling and control of flexible joint robots.

To the best of our knowledge the previous studies in the literature related to the control of parallel manipulators did not take joint flexibility into account. However consideration of joint flexibility in the controller design is especially important for parallel manipulators due to the high precision required in their applications. The aim of the present study is to develop an inverse dynamics motion control algorithm for parallel manipulators in the presence of flexibility at the joint drives. The system is first converted into an open-tree structure by disconnecting a sufficient number of unactuated joints. The closed loops are then expressed by constraint equations. It is shown that the acceleration level inverse dynamics equations form a singular set of differential equations because of the elastic media between the actuators and the end-effector. When the Lagrange multipliers and the intermediate variables are eliminated, a fourth-order input–output relation is obtained between the actuator torques and the end-effector position variables. The measured quantities are the positions and velocities of the actuated joints and rotors. Measurements of accelerations and jerks are not necessary. Damping which is inherent in the structural members used in drive trains is also considered in the dynamic model.

This paper is divided into six sections: The second section outlines the derivation of the dynamic equations of flexible joint parallel manipulators. In the third section, the inverse dynamics control method is introduced. Section 4 presents simulations of a three degree of freedom 2-RRR planar manipulator to illustrate the performance of the control algorithm. Discussions are given in Section 5. Conclusions form the last section.

2. Manipulator dynamics

Consider an n degree of freedom parallel manipulator. Let this system be converted into an open-tree structure by disconnecting a sufficient number of unactuated joints and the degree of freedom of the open-tree system be m, i.e., the number of independent loop closure constraints in the parallel manipulator be $m-n$. Let $\boldsymbol{\theta} = [\theta_1, \ldots, \theta_m]^{\mathrm{T}}$ denote the joint variables of the open system.

In the parallel manipulator as many joints as the degree of freedom of the manipulator are actuated. Let the joint variables be ordered such that the joint variable vector can be separated into two subvectors as $\boldsymbol{\theta}^{\mathrm{T}} = [\,\mathbf{q}^{\mathrm{T}} \quad \boldsymbol{\theta}^{u^{\mathrm{T}}}\,]$, where $\mathbf{q}$ is $n \times 1$ vector of the variables of the actuated joints and $\boldsymbol{\theta}^u$ is $(m-n) \times 1$ vector of the variables of the unactuated joints.

Due to the elasticity of the transmission elements, joint elasticity occurs at the actuated joints. The sources of elasticity are generally couplings, harmonic drives, and thin shafts used in drive trains. Joint elasticity of the power transmission elements at an actuated revolute joint is modelled as a torsional spring. Also structural damping of the transmission elements is modelled as a viscous torsional damper. For the ith transmission, k_i stands for the spring constant and d_i is used for the damping constant as seen in Fig. 1. The ith actuated joint variable q_i represents the angular position of the driven link of the manipulator with respect to the link on

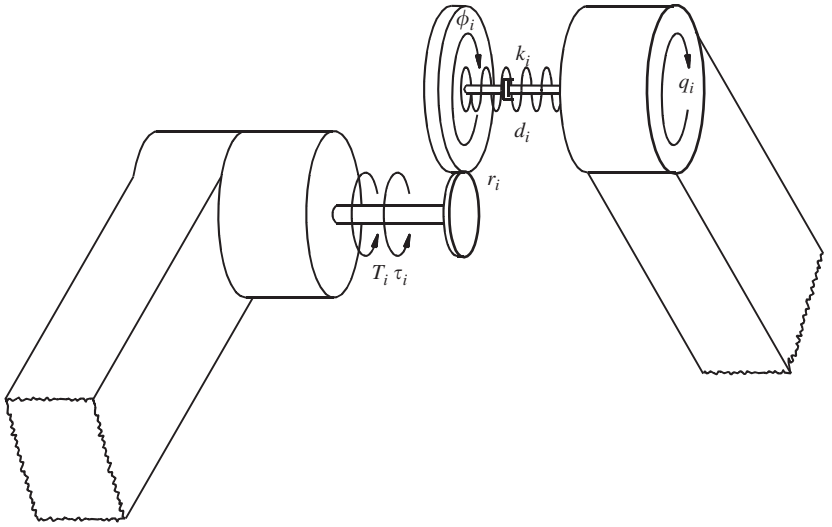

Fig. 1. Flexible joint drive.

which the ith actuator is mounted. The rotor angle of the ith actuator divided by the gear ratio r_i is denoted as the actuator variable ϕ_i. Then the vector of the actuator variables of the manipulator is $\boldsymbol{\varphi} = [\phi_1, \ldots, \phi_n]^{\mathrm{T}}$. The motor torques at the exit of the speed reductions are denoted by T_i, $i = 1, \ldots, n$. Elasticity at each of the actuated joints creates an additional degree of freedom in the system, with the rotors of the actuators being additional links. Hence the system has $2n$ degrees of freedom, while only n control actuator torques are available.

The open system is subject to the $m-n$ loop closure equations $g_i(\theta_1, \ldots, \theta_m) = 0$ which are obtained by reconnecting the disconnected joints. The number of the loop closure equations written for a disconnected joint is equal to the number of degrees of freedom restricted by that joint. The loop closure equations can be written at velocity level as

$$\mathbf{B}\dot{\boldsymbol{\theta}} = \mathbf{0} \tag{1}$$

where $\mathbf{B}(\boldsymbol{\theta})$ is the $(m-n) \times m$ constraint Jacobian matrix with $B_{ij} = \partial g_i / \partial \theta_j$, $i = 1, \ldots, m-n$, $j = 1, \ldots, m$.

It is assumed that the gear ratio r_i is large enough so that the kinetic energy of the rotor is due mainly to its own rotation [3]. In other words, the contribution of the angular velocities of the links to the rotational motion of the rotor is neglected. To see this, let ω_x, ω_y, ω_z be the angular velocity components of the link on which the actuator is mounted where the rotor angle is measured about the z-axis. The rotational kinetic energy of the ith actuator is written as $1/2\ [I_i^r(\omega_z + r_i\dot{\phi}_i)^2 + I_i^{r*}(\omega_x^2 + \omega_y^2)]$ where I_i^r is the moment of inertia of the ith rotor about its rotation axis and I_i^{r*} is the moment of inertia of the cylindrical rotor about the axes perpendicular to the rotation axis through the mass center. Since ω_x, ω_y, ω_z and $\dot{\phi}_i$ are in the same order of magnitude, the rotational kinetic energy of the rotor is approximately $\frac{1}{2} I_i^r r_i^2 \dot{\phi}_i^2$ if r_i is sufficiently large. By this assumption the inertia coupling terms between the joint and actuator variables disappear yielding the following equations of motion for the open-tree system of the parallel manipulator:

$$\mathbf{M}\ddot{\boldsymbol{\theta}} + \mathbf{Q} + \overline{\mathbf{D}} + \overline{\mathbf{K}} - \mathbf{B}^{\mathrm{T}}\boldsymbol{\lambda} = \mathbf{0} \tag{2}$$

$$\mathbf{I}^{\mathbf{r}}\ddot{\boldsymbol{\varphi}} - \mathbf{D}(\dot{\mathbf{q}} - \dot{\boldsymbol{\varphi}}) - \mathbf{K}(\mathbf{q} - \boldsymbol{\varphi}) = \mathbf{T} \tag{3}$$

where $\mathbf{M}(\boldsymbol{\theta})$ is the $m \times m$ symmetric positive definite generalized mass matrix and $\mathbf{Q}(\boldsymbol{\theta}, \dot{\boldsymbol{\theta}})$ is the $m \times 1$ vector which contains Coriolis, centrifugal and gravitational terms. $\mathbf{M}$ and $\mathbf{Q}$ are the same as those of the open system, which does not have joint elasticity where the rotor masses are included as part of the corresponding links.

$\overline{\mathbf{K}}$ is an $m \times 1$ vector which contains stiffness terms such that

$$\overline{\mathbf{K}} = \begin{bmatrix} \mathbf{K}(\mathbf{q} - \boldsymbol{\varphi}) \\ \mathbf{0} \end{bmatrix}$$

where $\mathbf{K}$ is $n \times n$ diagonal stiffness matrix with $K_{ii} = k_i$, $i = 1, \ldots, n$. Similarly $\overline{\mathbf{D}}$ is an $m \times 1$ vector which contains damping terms such that

$$\overline{\mathbf{D}} = \begin{bmatrix} \mathbf{D}(\dot{\mathbf{q}} - \dot{\boldsymbol{\varphi}}) \\ \mathbf{0} \end{bmatrix}$$

where $\mathbf{D}$ is $n \times n$ diagonal damping matrix with $D_{ii} = d_i$. $\mathbf{I}^r$ is $n \times n$ diagonal matrix of the rotor inertias where $I_{ii}^r = I_i^r r_i^2$, $i = 1, \ldots, n$. $\mathbf{T}$ is the $n \times 1$ vector of the motor torques at the exit of the speed reducers, $\mathbf{B}^{\mathrm{T}}\boldsymbol{\lambda}$ is the generalized constraint force vector and $\boldsymbol{\lambda}$ is the $(m-n) \times 1$ vector of Lagrange multipliers which represent the joint forces at the disconnected joints.

3. Inverse dynamics control

The control method to be used for the parallel manipulator is based on the relation between the inputs and the outputs. The inputs for the robot manipulator are the joint torques/forces (or voltages supplied to the actuators). Since end-effector position tracking is aimed in the control problem, the outputs are the end-effector position variables.

Let x_i, $i = 1, \ldots, n$ represent the Cartesian end-effector position variables. Then the functions that are used to relate each coordinate of the end-effector to the joint coordinates, i.e. so called task equations are written as $x_i = f_i(\theta_1, \ldots, \theta_m)$, $i = 1, \ldots, n$, and are expressed at velocity level as

$$\dot{\mathbf{x}} = \boldsymbol{\Gamma}\dot{\boldsymbol{\theta}} \tag{4}$$

where $\Gamma_{ij} = \partial f_i / \partial \theta_j$, $i = 1, \ldots, n$, $j = 1, \ldots, m$. Combining Eqs. (1) and (4), one can solve for $\dot{\boldsymbol{\theta}}$ from the assigned $\dot{\mathbf{x}}$ as

$$\dot{\boldsymbol{\theta}} = \mathbf{Z}^{-1}\mathbf{h} \tag{5}$$

where the $m \times m$ matrix $\mathbf{Z}$ is $\mathbf{Z}^{\mathrm{T}} = [\mathbf{B}^{\mathrm{T}} \quad \boldsymbol{\Gamma}^{\mathrm{T}}]$ and $\mathbf{h}^{\mathrm{T}} = [\mathbf{0} \quad \dot{\mathbf{x}}^{\mathrm{T}}]$.

At this point it is convenient to reduce the number of the dynamic equations by eliminating the unactuated joint accelerations $\ddot{\boldsymbol{\theta}}^u$ and the Lagrange multipliers $\boldsymbol{\lambda}$ in Eq (2) by making use of the constraint equations at acceleration level. To this end the constraint matrix is partitioned as $\mathbf{B} = [\mathbf{B}^a \quad \mathbf{B}^u]$ where the $(m-n) \times n$ matrix $\mathbf{B}^a$ and the $(m-n) \times (m-n)$ matrix $\mathbf{B}^u$ correspond to $\dot{\mathbf{q}}$ and $\dot{\boldsymbol{\theta}}^u$, respectively. Then $\dot{\boldsymbol{\theta}}^u$ can be written in terms of $\dot{\mathbf{q}}$ as below,

$$\mathbf{B}^u\dot{\boldsymbol{\theta}}^u = -\mathbf{B}^a\dot{\mathbf{q}} \tag{6}$$

Using the derivative of Eq. (6) with respect to time, one can solve for $\dot{\boldsymbol{\theta}}^u$ as

$$\ddot{\boldsymbol{\theta}}^u = -\mathbf{B}^{u^{-1}}[\mathbf{B}^a\ddot{\mathbf{q}} + \dot{\mathbf{B}}^a\dot{\mathbf{q}} + \dot{\mathbf{B}}^u\dot{\boldsymbol{\theta}}^u] \tag{7}$$

When $\mathbf{M}$ and $\mathbf{Q}$ are partitioned according to $\mathbf{q}$ and $\boldsymbol{\theta}^u$ as

$$\mathbf{M} = \begin{bmatrix} \mathbf{M}^{aa} & \mathbf{M}^{au} \\ \mathbf{M}^{au^{\mathrm{T}}} & \mathbf{M}^{uu} \end{bmatrix} \quad \text{and} \quad \mathbf{Q} = \begin{bmatrix} \mathbf{Q}^a \\ \mathbf{Q}^u \end{bmatrix}$$

Eq. (2) can be written as

$$\mathbf{M}^{aa}\ddot{\mathbf{q}} + \mathbf{M}^{au}\ddot{\boldsymbol{\theta}}^u + \mathbf{Q}^a + \mathbf{D}(\dot{\mathbf{q}} - \dot{\boldsymbol{\varphi}}) + \mathbf{K}(\mathbf{q} - \boldsymbol{\varphi}) - \mathbf{B}^{a^{\mathrm{T}}}\boldsymbol{\lambda} = \mathbf{0} \tag{8}$$

and

$$\mathbf{M}^{au^{\mathrm{T}}}\ddot{\mathbf{q}} + \mathbf{M}^{uu}\ddot{\boldsymbol{\theta}}^u + \mathbf{Q}^u - \mathbf{B}^{u^{\mathrm{T}}}\boldsymbol{\lambda} = \mathbf{0} \tag{9}$$

Substituting Eq. (7) into Eqs. (8) and (9), and then eliminating $\boldsymbol{\lambda}$ in the resulting equations, one obtains the following n dimensional equation:

$$\mathbf{M}^*\ddot{\mathbf{q}} + \mathbf{Q}^* + \mathbf{D}(\dot{\mathbf{q}} - \dot{\boldsymbol{\varphi}}) + \mathbf{K}(\mathbf{q} - \boldsymbol{\varphi}) = \mathbf{0} \tag{10}$$

where

$$\mathbf{M}^* = [\mathbf{M}^{aa} - \mathbf{M}^{au}\mathbf{B}^{u^{-1}}\mathbf{B}^a] - \mathbf{B}^{a^{\mathrm{T}}}(\mathbf{B}^{u^{-1}})^{\mathrm{T}}[\mathbf{M}^{au^{\mathrm{T}}} - \mathbf{M}^{uu}\mathbf{B}^{u^{-1}}\mathbf{B}^a] \tag{11}$$

and

$$\begin{aligned}\mathbf{Q}^* = {} & [-\mathbf{M}^{au}\mathbf{B}^{u^{-1}}\dot{\mathbf{B}}^a + \mathbf{B}^{a^{\mathrm{T}}}(\mathbf{B}^{u^{-1}})^{\mathrm{T}}\mathbf{M}^{uu}\mathbf{B}^{u^{-1}}\dot{\mathbf{B}}^a]\dot{\mathbf{q}} + [-\mathbf{M}^{au}\mathbf{B}^{u^{-1}}\dot{\mathbf{B}}^u \\ & + \mathbf{B}^{a^{\mathrm{T}}}(\mathbf{B}^{u^{-1}})^{\mathrm{T}}\mathbf{M}^{uu}\mathbf{B}^{u^{-1}}\dot{\mathbf{B}}^u]\dot{\boldsymbol{\theta}}^u + \mathbf{Q}^a - \mathbf{B}^{a^{\mathrm{T}}}(\mathbf{B}^{u^{-1}})^{\mathrm{T}}\mathbf{Q}^u\end{aligned} \tag{12}$$

$\boldsymbol{\Gamma}$ in the task equation (4) can be partitioned similarly to $\mathbf{B}$ as $\boldsymbol{\Gamma} = \begin{bmatrix}\boldsymbol{\Gamma}^a & \boldsymbol{\Gamma}^u\end{bmatrix}$, where the $n \times n$ matrix $\boldsymbol{\Gamma}^a$ and the $n \times (m-n)$ matrix $\boldsymbol{\Gamma}^u$ correspond to $\dot{\mathbf{q}}$ and $\dot{\boldsymbol{\theta}}^u$, respectively. Using Eqs. (6) and (7), $\ddot{\boldsymbol{\theta}}^u$ can be eliminated in the acceleration level task equations and the task equations can be written at acceleration level as

$$\mathbf{J}\ddot{\mathbf{q}} = -\dot{\mathbf{J}}\dot{\mathbf{q}} + \ddot{\mathbf{x}} \tag{13}$$

where $\mathbf{J} = \boldsymbol{\Gamma}^a - \boldsymbol{\Gamma}^u\mathbf{B}^{u^{-1}}\mathbf{B}^a$.

Eqs. (10), (3) and (13) constitute the inverse dynamic equations of the parallel manipulator from which the torques $\mathbf{T}$ can be obtained from the output vector $\mathbf{x}(t)$. These equations can be written in augmented form as

$$\begin{bmatrix}\mathbf{M}^* & \mathbf{0} & \mathbf{0} \\ \mathbf{0} & \mathbf{I}^r & -\mathbf{I} \\ \mathbf{J} & \mathbf{0} & \mathbf{0}\end{bmatrix}\begin{bmatrix}\ddot{\mathbf{q}} \\ \ddot{\boldsymbol{\varphi}} \\ \mathbf{T}\end{bmatrix} = \begin{bmatrix}-\mathbf{Q}^* - \mathbf{D}(\dot{\mathbf{q}} - \dot{\boldsymbol{\varphi}}) - \mathbf{K}(\mathbf{q} - \boldsymbol{\varphi}) \\ \mathbf{D}(\dot{\mathbf{q}} - \dot{\boldsymbol{\varphi}}) + \mathbf{K}(\mathbf{q} - \boldsymbol{\varphi}) \\ -\dot{\mathbf{J}}\dot{\mathbf{q}} + \ddot{\mathbf{x}}\end{bmatrix} \tag{14}$$

In fact, in the inverse dynamics problem the first and third rows of Eq. (14) involve the solution of the kinematic variables and can be termed as inverse kinematic equations of parallel manipulators with flexible joints. On the other hand, the second row of Eq. (14) is used for finding the control torques. Because of redundancy due to the joint flexibility, inertia and elastic force terms are also involved in the inverse kinematic equations, which can be expressed as

$$\begin{bmatrix}\mathbf{M}^* & \mathbf{0} \\ \mathbf{J} & \mathbf{0}\end{bmatrix}\begin{bmatrix}\ddot{\mathbf{q}} \\ \ddot{\boldsymbol{\varphi}}\end{bmatrix} = \begin{bmatrix}-\mathbf{Q}^* - \mathbf{D}(\dot{\mathbf{q}} - \dot{\boldsymbol{\varphi}}) - \mathbf{K}(\mathbf{q} - \boldsymbol{\varphi}) \\ -\dot{\mathbf{J}}\dot{\mathbf{q}} + \ddot{\mathbf{x}}\end{bmatrix} \tag{15}$$

However, Eq. (15) cannot be solved in this form since it is a singular set of differential equations. Hence, the acceleration level inverse dynamic equations (14) also represent a singular set of differential equations. The physical reason for the singularity is that because the control torques are transmitted to the end-effector through the elastic joints, then the control torques do not have an instantaneous effect on the end-effector acceleration.

When the intermediate variables $\boldsymbol{\varphi}$ and $\mathbf{q}$ are eliminated by manipulating the rows of Eq. (14), the relation between the input $\mathbf{T}$ and the output $\mathbf{x}$ is obtained as

$$\mathbf{N}\ddot{\mathbf{x}} + \mathbf{P} = \mathbf{T} + \mathbf{S}\dot{\mathbf{T}} \tag{16}$$

where

$$\mathbf{N} = \mathbf{K}^{-1}\mathbf{I}^r\mathbf{M}^*\mathbf{J}^{-1} \tag{17}$$

$$\mathbf{S} = \mathbf{K}^{-1}\mathbf{D} \tag{18}$$

and

$$\begin{aligned}\mathbf{P} = {} & \mathbf{K}^{-1}\mathbf{I}^r[(-3\mathbf{M}^*\mathbf{J}^{-1}\dot{\mathbf{J}} + 2\dot{\mathbf{M}}^* + \mathbf{D})\ddot{\mathbf{q}} + (-3\mathbf{M}^*\mathbf{J}^{-1}\ddot{\mathbf{J}} + \ddot{\mathbf{M}}^* + \mathbf{K})\dot{\mathbf{q}} \\ & + (-\mathbf{M}^*\mathbf{J}^{-1}\dddot{\mathbf{J}})\mathbf{q} + \dddot{\mathbf{Q}}^*] + \mathbf{K}^{-1}\mathbf{D}[\mathbf{M}^*\ddot{\mathbf{q}} + \dot{\mathbf{M}}^*\dot{\mathbf{q}} + \ddot{\mathbf{Q}}^*] + \mathbf{M}^*\ddot{\mathbf{q}} + \mathbf{Q}^*\end{aligned} \tag{19}$$

Eq. (16) shows that the control torques have an instantaneous effect on the end-effector snaps (second derivatives of the end-effector accelerations). An inverse dynamics control law can be formulated by choosing control torques which will linearize and decouple the system. To this end $\mathbf{T}+\mathbf{S}\dot{\mathbf{T}}$ is chosen as

$$\mathbf{T}+\mathbf{S}\dot{\mathbf{T}}=\mathbf{N}\mathbf{u}+\mathbf{P} \tag{20}$$

where $\mathbf{u}$ is $n\times 1$ control input vector that represents the command snaps

$$\mathbf{u}=\dddot{\mathbf{x}}^{d}+\mathbf{C}_1(\ddot{\mathbf{x}}^{d}-\ddot{\mathbf{x}})+\mathbf{C}_2(\dddot{\mathbf{x}}^{d}-\dddot{\mathbf{x}})+\mathbf{C}_3(\dot{\mathbf{x}}^{d}-\dot{\mathbf{x}})+\mathbf{C}_4(\mathbf{x}^{d}-\mathbf{x}) \tag{21}$$

the superscript d is used for the desired values and $\mathbf{C}_i$, $i=1,\ldots,4$ are diagonal feedback gain matrices. Once $\mathbf{T}+\mathbf{S}\dot{\mathbf{T}}$ is obtained from Eq. (16), T can be found by numerical integration. Note that if joint damping is neglected, $\mathbf{S}$ in Eqs. (16) and (20) vanishes. In the absence of any modelling error, the actual snaps produced by these control torques, are equal to the command snaps, i.e. $\dddot{\mathbf{x}}=\mathbf{u}$. Using Eq. (21), this leads to the following linear and decoupled error dynamics

$$\ddddot{\mathbf{e}}+\mathbf{C}_1\dddot{\mathbf{e}}+\mathbf{C}_2\ddot{\mathbf{e}}+\mathbf{C}_3\dot{\mathbf{e}}+\mathbf{C}_4\mathbf{e}=0 \tag{22}$$

where $\mathbf{e}=\mathbf{x}^{d}-\mathbf{x}$. Asymptotic stability is achieved by appropriate choice of the feedback gains C_{ijj}, $i=1,\ldots,4$, $j=1,\ldots,n$.

The necessary measurements for the calculation of the control torques are the positions and velocities of the actuated joints and the actuator rotors, i.e. $\mathbf{q}$, $\dot{\mathbf{q}}$, $\boldsymbol{\varphi}$ and $\dot{\boldsymbol{\varphi}}$. The remaining variables that appear in the control law are calculated using these quantities. The joint acceleration vector $\ddot{\mathbf{q}}$ is calculated using Eq. (10) and the joint jerk vector $\dddot{\mathbf{q}}$ is found using the derivative of Eq. (10) in which $\ddot{\boldsymbol{\varphi}}$ is inserted by making use of Eq. (3), i.e.

$$\dddot{\mathbf{q}}=-\mathbf{M}^{*-1}\{\dot{\mathbf{M}}^{*}\ddot{\mathbf{q}}+\dot{\mathbf{Q}}^{*}+\mathbf{D}\ddot{\mathbf{q}}-\mathbf{D}\mathbf{I}^{r-1}[\mathbf{D}(\dot{\mathbf{q}}-\dot{\boldsymbol{\varphi}})-\mathbf{K}(\mathbf{q}-\boldsymbol{\varphi})-\mathbf{T}]+\mathbf{K}(\dot{\mathbf{q}}-\dot{\boldsymbol{\varphi}})\} \tag{23}$$

The unactuated joint variable states $\boldsymbol{\theta}^{u}$, $\dot{\boldsymbol{\theta}}^{u}$, $\ddot{\boldsymbol{\theta}}^{u}$ and $\dddot{\boldsymbol{\theta}}^{u}$ are obtained using the loop closure equations and their derivatives and the end-effector states $\mathbf{x}$, $\dot{\mathbf{x}}$, $\ddot{\mathbf{x}}$ and $\dddot{\mathbf{x}}$ are found from the task equations and their derivatives.

Parallel manipulators with rigid joints possess kinematic and drive singular positions. In addition to the numerical problems that occur at such positions, passing through such positions is in general not possible unless certain consistency conditions are satisfied [16]. At a kinematic singular position the assigned end-effector motion cannot in general be reached by the manipulator (the manipulator loses one or more degrees of freedom) and at a drive singular position the actuators lose control of the manipulator in certain directions (the actuators lose control of one or more degrees of freedom). Kinematic singularities occur when $\mathbf{Z}$ is singular and drive singularities occur when $\mathbf{B}^{u}$ is singular [16,17]. As seen in Eqs. (5) and (7) the same singularity conditions occur in the presence of joint flexibility. In this paper, it is assumed that the end-effector trajectory is chosen such that the manipulator never comes to a kinematic or drive singular position, i.e. $\mathbf{Z}$ and $\mathbf{B}^{u}$ are always nonsingular.

4. Case study

A planar parallel manipulator shown in Fig. 2 is considered as a case study in order to check the performance of the control law. Parallel manipulators are generally classified according to the number of legs and the types of joints that their legs have beginning from the fixed base to the moving platform. The parallel manipulator to be analyzed has two legs and each of them has three revolute joints from the fixed base to the moving platform.

The manipulator has three degrees of freedom, i.e. $n=3$, excluding the additional degrees of freedom that arise due to the flexible joints. Let the manipulator be actuated by three actuators located at joints A, B and C whose joint variables are θ_1, θ_2 and θ_3.

For this particular numerical example, considering disconnection of the revolute joint at F, $m=5$ and the vector of the joint variables of the open system is

$$\boldsymbol{\theta}=\begin{bmatrix}\theta_1 & \theta_2 & \theta_3 & \theta_4 & \theta_5\end{bmatrix}^{\mathrm{T}} \tag{24}$$

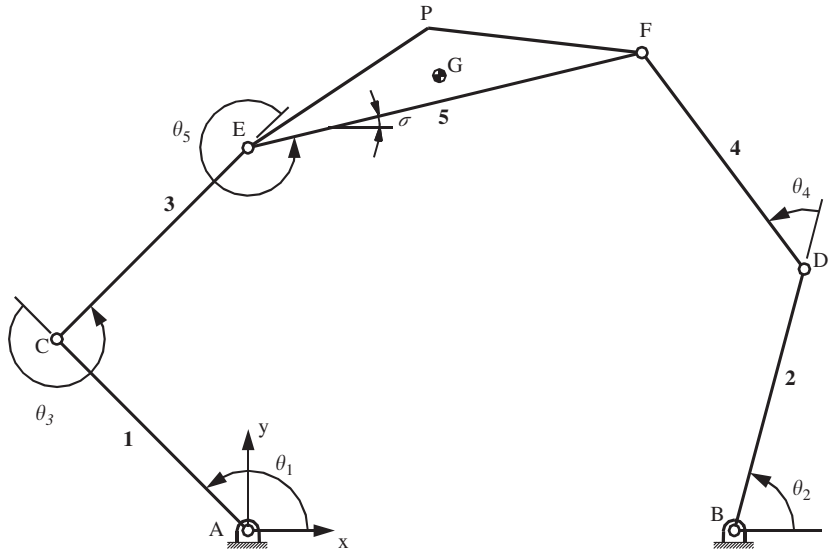

Fig. 2. 2-RRR parallel manipulator.

which is subdivided into the vectors of the actuated and the unactuated joint variables as

$$\mathbf{q} = \begin{bmatrix} \theta_1 & \theta_2 & \theta_3 \end{bmatrix}^{\mathrm{T}} \tag{25}$$

$$\boldsymbol{\theta}^u = \begin{bmatrix} \theta_4 & \theta_5 \end{bmatrix}^{\mathrm{T}} \tag{26}$$

The vector of the actuator variables becomes

$$\boldsymbol{\varphi} = \begin{bmatrix} \phi_1 & \phi_2 & \phi_3 \end{bmatrix}^{\mathrm{T}} \tag{27}$$

The fixed dimensions of the manipulator are labeled as $L_1 = AC$, $L_2 = BD$, $L_3 = CE$, $L_4 = DF$, $L_5 = EF$, $d_o = AB$, $a = \angle PEF$, $b = \angle GEF$, $g_5 = GE$ and $d_5 = EP$. Links 1–4 are uniform bars. The numerical data are $L_1 = L_2 = L_3 = L_4 = 1.0\,m$, $L_5 = 1.5\,m$, $d_o = 1.8\,m$, $g_5 = 0.75\,m$, $d_5 = 0.8\,m$, $\alpha = 20^\circ$ and $\beta = 7^\circ$. The masses of the links are $m_1^L = m_2^L = m_3^L = m_4^L = 10\,\mathrm{kg}$ and $m_5^L = 15\,\mathrm{kg}$. The motors and speed reducers at the active joints have small dimensions compared to the links. The combined mass of the motor and the speed reducer mounted on link-1 is $m_3^A = 1.2\,\mathrm{kg}$. The rotor moments of inertia about respective axes are $I_1^r = 7.0\text{e}{-05}\,\mathrm{kg\,m^2}$, $I_2^r = 8.0\text{e}{-05}\,\mathrm{kg\,m^2}$, $I_3^r = 9.0\text{e}{-05}\,\mathrm{kg\,m^2}$. The gear ratios are $r_1 = r_2 = r_3 = 100$. Spring constants at the actuated joints are $k_1 = k_2 = k_3 = 5000\,\mathrm{N\,m/rad}$. Structural damping constants of the actuated joints correspond to a 3% damping ratio for the structural vibration of each rotor, i.e. $d_1 = 0.0355\,\mathrm{N\,m\,s/rad}$, $d_2 = 0.0379\,\mathrm{N\,m\,s/rad}$, $d_3 = 0.0402\,\mathrm{N\,m\,s/rad}$.

The task variables are the coordinates of point P on the moving platform and the orientation of the moving platform, i.e. $\mathbf{x} = [\,x_P \quad y_P \quad \sigma\,]^{\mathrm{T}}$. The moving platform is assumed to make the following deployment motion:

$$x_p^d = \begin{cases} 0.70 + \dfrac{0.5}{T}\left[t - \dfrac{T}{2\pi}\sin\dfrac{2\pi t}{T}\right]m & 0 \leqslant t \leqslant T \\ 1.20\,m & t > T \end{cases} \tag{28a}$$

$$y_p^d = \begin{cases} 1.90 - \dfrac{0.5}{T}\left[t - \dfrac{T}{2\pi}\sin\dfrac{2\pi t}{T}\right]m & 0 \leqslant t \leqslant T \\ 1.40\,m & t > T \end{cases} \tag{28b}$$

$$\sigma^d = \begin{cases} 15 + \dfrac{20}{T}[t - \dfrac{T}{2\pi}\sin\dfrac{2\pi t}{T}]\,deg & 0 \leqslant t \leqslant T \\ 35\,deg & t > T \end{cases} \tag{28c}$$

where T is the period of the deployment motion and selected as $T = 0.6$ s. $\mathbf{M}$ and $\mathbf{Q}$ of the dynamic equations, the loop closure equations and the task equations are given in the appendix.

The kinematic singular positions are obtained from $|\mathbf{Z}| = 0$ as the positions where $\theta_3 = \pm k\pi$ or $\theta_4 = \pm k\pi$ ($k = 0, 1, 2, \ldots$), i.e. when links 1 and 3 or links 2 and 4 are in folded or extended positions. On the other hand the drive singular positions are obtained from $|\mathbf{B}^u| = 0$ as the positions where $(\theta_1 + \theta_3 + \theta_5 - \theta_2 - \theta_4) = \pm k\pi$ ($k = 0, 1, 2, \ldots,$), i.e. when points E, F and D become collinear [18]. The specified end-effector trajectory does not involve any of these singular configurations.

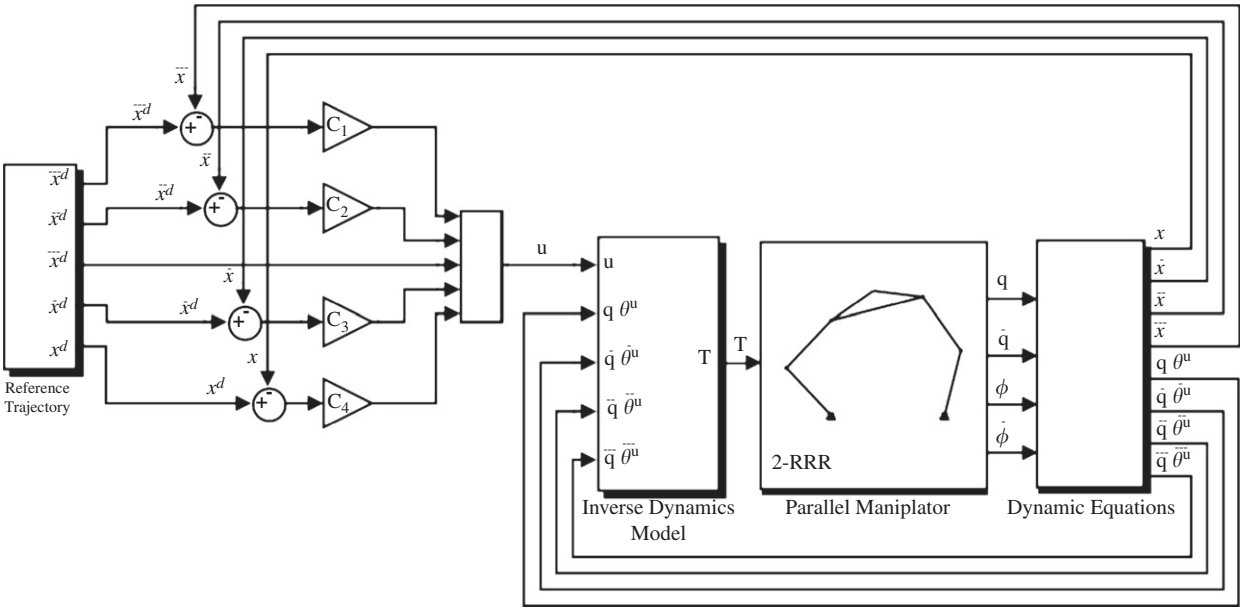

Fig. 3. Implementation of inverse dynamics control scheme.

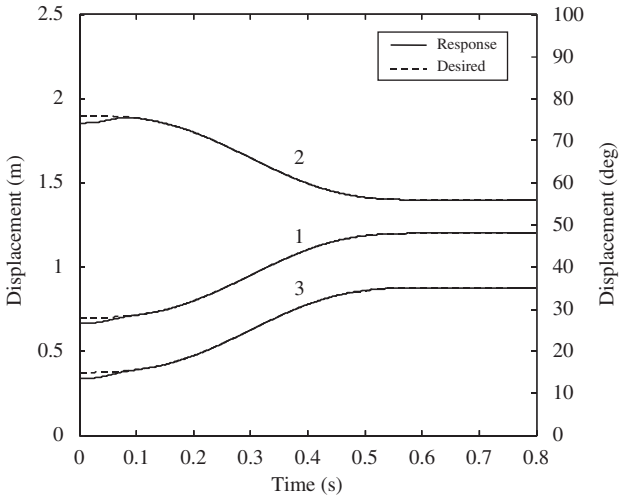

Fig. 4. Position response: (1) x_P, (2) y_P and (3) σ.

The parallel manipulator is assumed to be at rest initially and have the following initial active joint positions as $\theta_{1o} = 135^\circ$, $\theta_{2o} = 75^\circ$, $\theta_{3o} = -90^\circ$. The corresponding initial passive joint angles are $\theta_{4o} = 51.91^\circ$, $\theta_{5o} = -31.46^\circ$, and the task space initial positions are $x_{1o} = 0.6668\,\text{m}$, $x_{2o} = 1.8563\,\text{m}$, $x_{3o} = 13.55^\circ$. Hence the initial position is chosen to have an initial position error. In addition, the cycloidal motion profile is continuous up to the acceleration level but has discontinuous jerks at the boundaries.

The feedback gain diagonal matrices $\mathbf{C}_i$, $i = 1, \ldots, 4$ are chosen to satisfy ITAE performance criteria, i.e. $C_{1jj} = 2.1\omega_{oj}$, $C_{2jj} = 3.4{\omega_{oj}}^2$, $C_{3jj} = 2.7{\omega_{oj}}^3$, $C_{4jj} = {\omega_{oj}}^4$, $j = 1, 2, 3$ where ω_{oj} are positive constants. With these gains the two natural frequencies of the closed-loop error dynamics in each direction are $0.75\omega_{oj}$ and $1.33\omega_{oj}$.

The control torques as obtained from Eq. (20) are applied to the system represented by Eqs. (10) and (3) for the forward dynamics solution. The values obtained for $\ddot{\mathbf{q}}$ and $\ddot{\boldsymbol{\varphi}}$ using these equations are numerically integrated to obtain $\mathbf{q}$, $\dot{\mathbf{q}}$, $\boldsymbol{\varphi}$ and $\dot{\boldsymbol{\varphi}}$ which are taken as the measured quantities. Then the actuated joint acceleration and jerk vectors $\ddot{\mathbf{q}}$ and $\dddot{\mathbf{q}}$ are calculated using Eqs. (10) and (23) in which the parameters contain modelling error, if any. Matlab® and one of its integrated tools Simulink® are used for the simulation. The implementation of the control system is shown in Fig. 3. In the simulations $\omega_{oj} = 50\,\text{rad/s}$, $j = 1, 2, 3$ and the sampling time interval $h = 0.002\,\text{s}$.

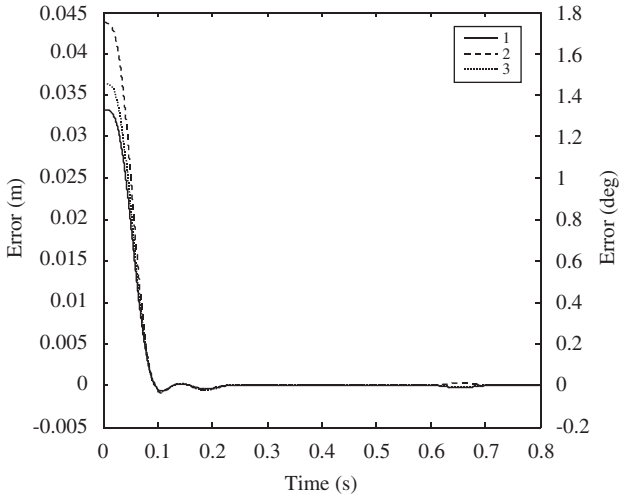

Fig. 5. Position errors: (1) $x_P - x_P{}^d$, (2) $y_P - y_P{}^d$ and (3) $\sigma - \sigma^d$.

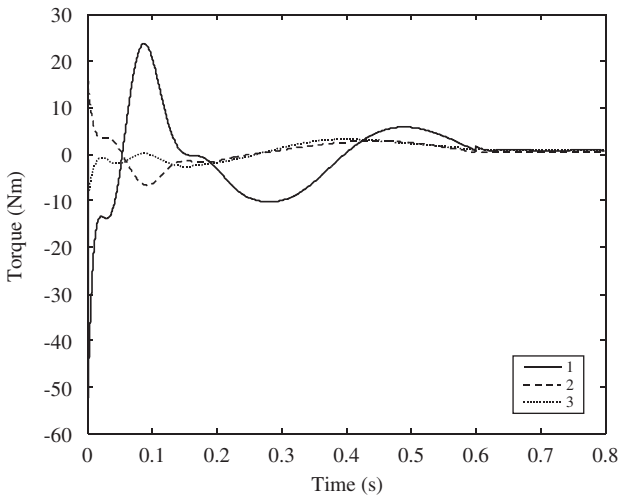

Fig. 6. Control torques: (1) T_1, (2) T_2 and (3) T_3.

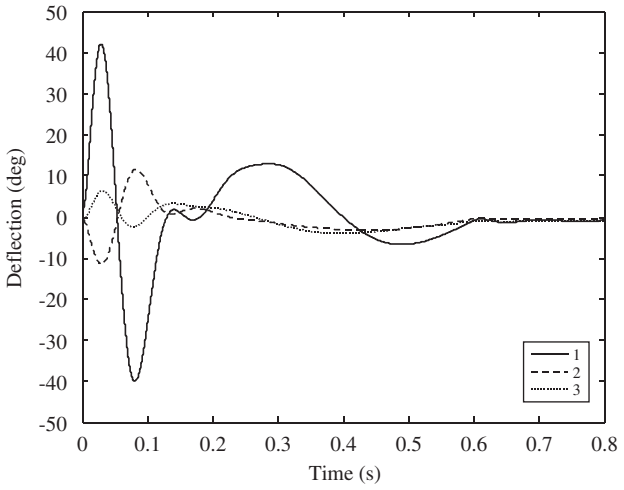

Fig. 7. Deflections: (1) $\theta_1-\phi_1$, (2) $\theta_2-\phi_2$ and (3) $\theta_3-\phi_3$.

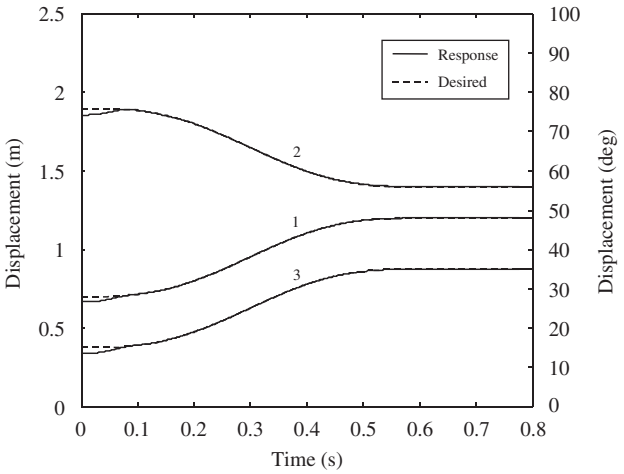

Fig. 8. Position response (modelling error): (1) x_P, (2) y_P and (3) σ.

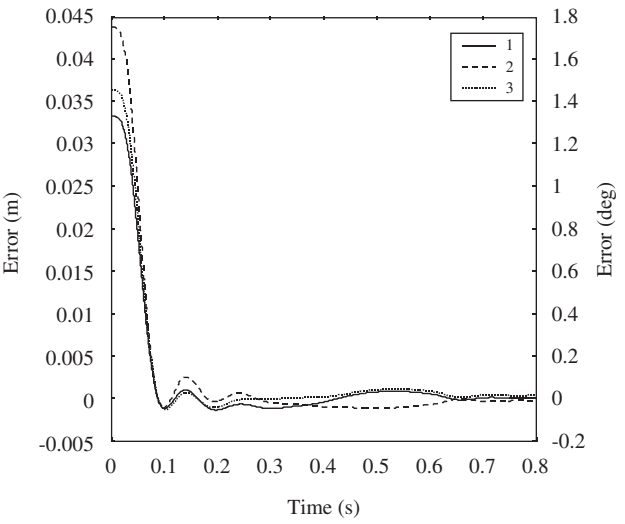

Fig. 9. Position errors (modelling error): (1) $x_P-x_P{}^d$, (2) $y_P-y_P{}^d$ and (3) $\sigma-\sigma^d$.

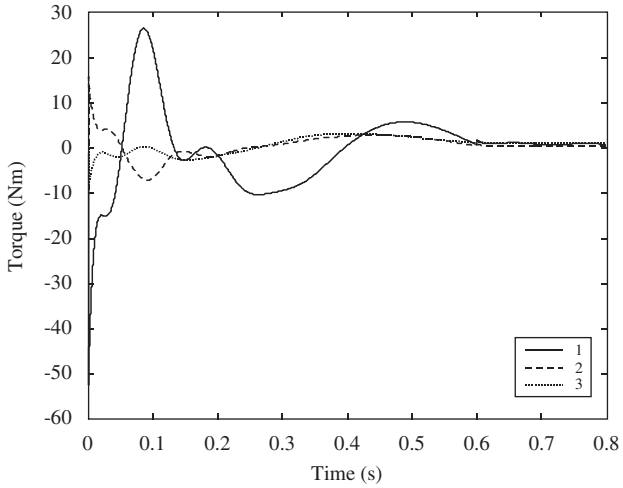

Fig. 10. Control torques (modelling error): (1) T_1, (2) T_2 and (3) T_3.

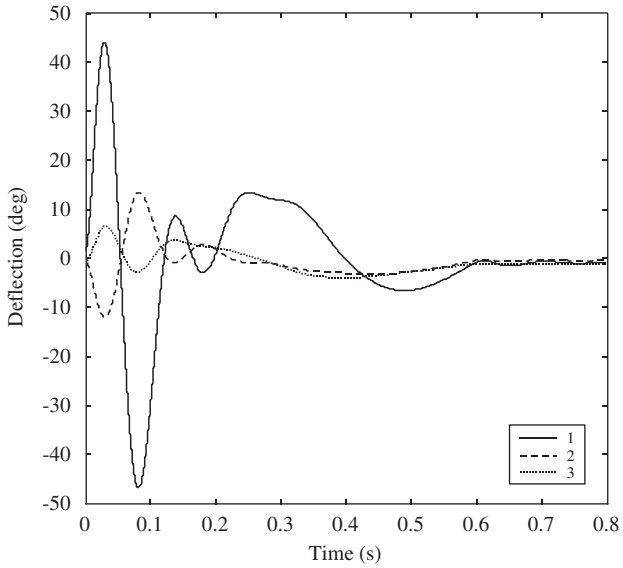

Fig. 11. Deflections (modelling error): (1) $\theta_1-\phi_1$, (2) $\theta_2-\phi_2$ and (3) $\theta_3-\phi_3$.

The closed-loop response and the errors are shown in Figs. 4 and 5, respectively. It is seen that good tracking properties are achieved at all task variables. The control torques are plotted in Fig. 6 and the elastic deflections in Fig. 7. The initial and final elastic deflections are nonzero due to the gravitational forces.

To see the effects of modelling error the closed-loop system is also simulated using 10% smaller values for the inertia and elastic properties in the model. The response and the errors are shown in Figs. 8 and 9, respectively. The steady state errors are observed to be quite small. Figs. 10 and 11 show the control torques and the elastic deflections respectively in the presence of modelling error.

5. Discussions

The control law developed yielded good tracking properties even in the presence of modelling error. The errors can further be decreased if higher ω_{oj} are used.

The sampling frequency are chosen to be not less than 10 times the largest natural frequency of the closed-loop system. When smaller sampling frequencies are used, instability and divergence of the control torques and response are observed. Hence, the controller bandwidth can be increased by increasing the sampling frequency. On the other hand the real time computational requirements place an upper limit on the sampling frequency.

In the paper the motor dynamics are not considered in order to concentrate on the dynamics of the flexible joint parallel manipulators. Hence it is assumed that the required control torques are applied without any delay. This assumption is justified if brushless DC motors are used which are popular in robot applications. The frequency response of the current loop in brushless DC motors is wide enough to minimize any effect on outer control loops and hence the motor dynamics are not considered [20].

Parallel manipulators possess drive singular positions in addition to the kinematic singular positions that serial manipulators also have. At kinematic singular positions, the manipulator loses one or more degrees of freedom and at drive singular positions the actuators lose the control of one or more degrees of freedom. It is possible to utilize consistency conditions and modified dynamic equations near singular positions [16,19]. However, in the present study the singular positions are avoided in the motion planning stage for the sake of simplicity.

6. Conclusions

It is shown that in a flexible joint parallel manipulator the actuator forces do not have an instantaneous effect on the end-effector accelerations due to the elastic media. To find the input–output relation, first the loop closure constraint equations are utilized to eliminate the unactuated joint variables and the Lagrange multipliers. Then the resulting dynamic equations are manipulated to eliminate the actuator variables yielding a fourth-order relation between the actuator torques and the end-effector position variables. Joint structural damping is also considered in the dynamic model, which brings an additional complexity due to the appearance of the torque rates in the input output relation. The inverse dynamics control law developed decouples and linearizes the system, yielding asymptotically stable fourth-order error dynamics by feedback of positions and velocities of the actuated joints and rotors. Measurements of the joint accelerations and jerks are not necessary since they are calculated from the dynamic equations.

Appendix

The elements of **M** and **Q** shown in Eq. (2) are given below, where m_i, $i=1,\ldots,5$ are the masses of the links, I_{izz}, $i=1,\ldots,5$ are the centroidal moments of inertia of the links and $c\theta_{ijk}=\cos(\theta_i+\theta_j+\theta_k)$, $s\theta_{ijk}=\sin(\theta_i+\theta_j+\theta_k)$.

$$M_{11}=\left[m_1^L\frac{L_1^2}{4}+I_{1zz}\right]+m_3^L L_1^2+m_3^L L_1 L_3 c\theta_3+\left[m_3^L\frac{L_3^2}{4}+I_{3zz}\right]+m_5^L L_1^2+m_5^L L_3^2 + [m_5^L g_5^2+I_{5zz}]+2m_5^L L_1 L_3 c\theta_3+2m_5^L L_1 g_5 c(\theta_{35}+\beta)+2m_5^L L_3 g_5 c(\theta_5+\beta)+m_3^A L_1^2 \tag{A.1}$$

$$M_{13}=\frac{1}{2}m_3^L L_1 L_3 c\theta_3+\left[m_3^L\frac{L_3^2}{4}+I_{3zz}\right]+m_5^L L_3^2+[m_5^L g_5^2+I_{5zz}]+m_5^L L_1 L_3 c\theta_3 + m_5^L L_1 g_5 c(\theta_{35}+\beta)+2m_5^L L_3 g_5 c(\theta_5+\beta) \tag{A.2}$$

$$M_{15}=[m_5^L g_5^2+I_{5zz}]+m_5^L L_1 g_5 c(\theta_{35}+\beta)+m_5^L L_3 g_5 c(\theta_5+\beta) \tag{A.3}$$

$$M_{22}=\left[m_2^L\frac{L_2^2}{4}+I_{2zz}\right]+m_4^L L_2^2+m_4^L L_2 L_4 c\theta_4+\left[m_4^L\frac{L_4^2}{4}+I_{4zz}\right] \tag{A.4}$$

$$M_{24}=\frac{1}{2}m_4^L L_2 L_4 c\theta_4+\left[m_4^L\frac{L_4^2}{4}+I_{4zz}\right] \tag{A.5}$$

$$M_{33} = \left[m_3^L \frac{L_3^2}{4} + I_{3zz}\right] + m_5^L L_3^2 + [m_5^L g_5^2 + I_{5zz}] + 2m_5^L L_3 g_5 c(\theta_5 + \beta) \tag{A.6}$$

$$M_{35} = [m_5^L g_5^2 + I_{5zz}] + m_5^L L_3 g_5 c(\theta_5 + \beta) \tag{A.7}$$

$$M_{44} = \left[m_4^L \frac{L_4^2}{4} + I_{4zz}\right] \tag{A.8}$$

$$M_{55} = [m_5^L g_5^2 + I_{5zz}] \tag{A.9}$$

$$Q_1 = m_1^L g \frac{L_1}{2} c\theta_1 + m_3^L g\left(L_1 c\theta_1 + \frac{L_3}{2} c\theta_{13}\right) + m_5^L g\left[L_1 c\theta_1 + L_3 c\theta_{13} + g_5 c(\theta_{135} + \beta)\right] + m_3^A g L_1 c\theta_1 \tag{A.10}$$

$$Q_2 = m_2^L g\left(\frac{L_2}{2} c\theta_2\right) + m_4^L g\left(L_2 c\theta_2 + \frac{L_4}{2} c\theta_{24}\right) \tag{A.11}$$

$$\begin{aligned} Q_3 = {} & \frac{1}{2}\dot{\theta}_1^2[m_3^L L_1 L_3 s\theta_3 + 2m_5^L L_1 L_3 s\theta_3 + 2m_5^L L_1 g_5 s(\theta_{35} + \beta)] \\ & + \dot{\theta}_1\dot{\theta}_3\left[\frac{1}{2} m_3^L L_1 L_3 s\theta_3 + m_5^L L_1 L_3 s\theta_3 + m_5^L L_1 g_5 s(\theta_{35} + \beta)\right] \\ & + \dot{\theta}_1\dot{\theta}_5[m_3^L L_1 g_5 s(\theta_{35} + \beta)] + m_3^L g\left(\frac{L_3}{2} c\theta_{13}\right) + m_5^L g[L_3 c\theta_{13} + g_5 c(\theta_{135} + \beta)] \end{aligned} \tag{A.12}$$

$$Q_4 = \frac{1}{2}\dot{\theta}_2^2 m_4^L L_2 L_4 s\theta_4 + \dot{\theta}_2\dot{\theta}_4 \frac{1}{2} m_4^L L_2 L_4 s\theta_4 + m_2^L g\left(\frac{L_2}{2} c\theta_2\right) + m_4^L g\left(L_2 c\theta_2 + \frac{L_4}{2} c\theta_{24}\right) \tag{A.13}$$

$$\begin{aligned} Q_5 = {} & \dot{\theta}_1^2[m_5^L L_1 g_5 s(\theta_{35} + \beta) + m_5^L L_3 g_5 s(\theta_5 + \beta)] + \dot{\theta}_3^2 m_5^L L_3 g_5 s(\theta_5 + \beta) \\ & + \dot{\theta}_1\dot{\theta}_3[m_5^L L_1 g_5 s(\theta_{35} + \beta) + 2m_5^L L_3 g_5 s(\theta_5 + \beta)] + \dot{\theta}_1\dot{\theta}_5[m_5^L L_1 g_5 s(\theta_{35} + \beta) \\ & + m_5^L L_3 g_5 s(\theta_5 + \beta)] + \dot{\theta}_3\dot{\theta}_5 m_5^L L_3 g_5 s(\theta_5 + \beta) + m_5^L g[g_5 c(\theta_{135} + \beta)] \end{aligned} \tag{A.14}$$

Then the submatrices of **M** and **Q** are

$$\mathbf{M}^{aa} = \begin{bmatrix} M_{11} & 0 & M_{13} \\ 0 & M_{22} & 0 \\ M_{31} & 0 & M_{33} \end{bmatrix}, \quad \mathbf{M}^{au} = \mathbf{M}^{ua^{\mathrm{T}}} = \begin{bmatrix} 0 & M_{15} \\ M_{24} & 0 \\ 0 & M_{35} \end{bmatrix}, \quad \mathbf{M}^{uu} = \begin{bmatrix} M_{44} & 0 \\ 0 & M_{55} \end{bmatrix} \tag{A.15}$$

$$\mathbf{Q}^{a^{\mathrm{T}}} = \begin{bmatrix} Q_1 & Q_2 & Q_3 \end{bmatrix}, \quad \mathbf{Q}^{u^{\mathrm{T}}} = \begin{bmatrix} Q_4 & Q_5 \end{bmatrix} \tag{A.16}$$

The loop closure equations are given below:

$$g_1 = L_1 c\theta_1 + L_3 c\theta_{13} + L_5 c\theta_{135} - L_2 c\theta_2 - L_4 c\theta_{24} - d_0 = 0 \tag{A.17}$$

$$g_2 = L_1 s\theta_1 + L_3 s\theta_{13} + L_5 s\theta_{135} - L_2 s\theta_2 - L_4 s\theta_{24} = 0 \tag{A.18}$$

Then the submatrices of **B** take the following form:

$$\mathbf{B}^a = \begin{bmatrix} -L_1 s\theta_1 - L_3 s\theta_{13} - L_5 s\theta_{135} & L_2 s\theta_2 + L_4 s\theta_{24} & -L_3 s\theta_{13} - L_5 s\theta_{135} \\ L_1 c\theta_1 + L_3 c\theta_{13} + L_5 c\theta_{135} & -L_2 c\theta_2 - L_4 c\theta_{24} & L_3 c\theta_{13} + L_5 c\theta_{135} \end{bmatrix} \tag{A.19}$$

$$\mathbf{B}^u = \begin{bmatrix} L_4 s\theta_{24} & -L_5 s\theta_{135} \\ -L_4 c\theta_{24} & L_5 c\theta_{135} \end{bmatrix} \tag{A.20}$$

The task equations are as follows:

$$f_1 = x_P = L_1 c\theta_1 + L_3 c\theta_{13} + d_5 c(\theta_{135} + \alpha) \tag{A.21}$$

$$f_2 = y_P = L_1 s\theta_1 + L_3 s\theta_{13} + d_5 s(\theta_{135} + \alpha) \tag{A.22}$$

$$f_3 = \sigma = \theta_{135} \tag{A.23}$$

The submatrices of $\mathbf{\Gamma}$ are

$$\mathbf{\Gamma}^a = \begin{bmatrix} -L_1 s\theta_1 - L_3 s\theta_{13} - d_5 s(\theta_{135} + \alpha) & 0 & -L_3 s\theta_{13} - d_5 s(\theta_{135} + \alpha) \\ L_1 c\theta_1 + L_3 c\theta_{13} + d_5 c(\theta_{135} + \alpha) & 0 & L_3 c\theta_{13} + d_5 c(\theta_{135} + \alpha) \\ 1 & 0 & 1 \end{bmatrix} \tag{A.24}$$

$$\mathbf{\Gamma}^u = \begin{bmatrix} 0 & -d_5 s(\theta_{135} + \alpha) \\ 0 & d_5 c(\theta_{135} + \alpha) \\ 0 & 1 \end{bmatrix} \tag{A.25}$$

References

[1] E.I. Rivin, Compliance breakdown for robot structures, *Proceedings of the Symposium Engineering Applied Mechanics*, Toronto, 1984, pp. 55–67.

[2] M.C. Good, L.M. Sweet, K.L. Strobel, Dynamic models for control system design of integrated robot and drive systems, *Journal of Dynamic Systems, Measurement and Control* 107 (1985) 53–59.

[3] M.W. Spong, Modeling and control of elastic joint robots, *Journal of Dynamic Systems Measurement and Control* 109 (1987) 310–319.

[4] M.G. Forrest-Barlach, S.M. Babcock, Inverse dynamics task control of a compliant manipulator, *IEEE Journal of Robotics and Automation* 3 (1987) 75–83.

[5] K.P. Jankowski, H. Van Brussel, An approach to discrete inverse dynamics control of flexible joint robots, *IEEE Journal of Robotics and Automation* 8 (1992) 651–658.

[6] S.K. Ider, M.K. Özgören, Trajectory tracking control of flexible joint robots, *Computers and Structures* 76 (2000) 757–763.

[7] F. Ghorbel, M.W. Spong, Integral manifolds of singularly perturbed systems with application to rigid-link flexible-joint multibody systems, *International Journal of Non-linear Mechanics* 35 (2000) 133–155.

[8] S.K. Ider, Force and motion trajectory tracking control of flexible-joint robots, *Mechanism and Machine Theory* 35 (2000) 363–378.

[9] Y.R. Hu, G. Vukovich, Position and force control of flexible joint robots during constrained motion tasks, *Mechanism and Machine Theory* 36 (2001) 853–871.

[10] K.P. Jankowski, H.A. Elmaraghy, Inverse dynamics and feedforward controllers for high precision position/force tracking of flexible joint robots, *Robotica* 12 (1994) 227–241.

[11] R.A. Al Ashoor, R.V. Patel, K. Khorasani, Robust adaptive controller design and stability for flexible joint robots, *IEEE Transactions on Systems, Man and Cybernetics* 23 (1993) 589–602.

[12] A.C. Huang, Y.C. Chen, Adaptive sliding control for single link flexible joint robots with mismatched uncertainties, *IEEE Transactions on Control System Technology* 12 (2004) 770–776.

[13] C.J. Tsaprounis, N.A. Asparagathos, Adaptive tractive controller for rigid link elastic joint robots with link acceleration estimation, *Journal of Intelligent and Robotic Systems* 27 (2000) 67–83.

[14] S. Ozgoli, H.D. Taghirad, A survey on the control of flexible joint robots, *Asian Journal of Control* 8 (2006) 1–15.

[15] S.K. Dwivedy, P. Eberhard, Dynamic analysis of flexible manipulators, a literature review, *Mechanism and Machine Theory* 41 (2006) 749–777.

[16] S.K. Ider, Inverse dynamics of parallel manipulators in the presence of drive singularities, *Mechanism and Machine Theory* 40 (2005) 33–44.

[17] Z. Ji, Study of three degree of freedom 2-RRR parallel manipulators, *Mechanism and Machine Theory* 38 (2003) 409–416.

[18] O. Korkmaz, Inverse dynamics control of flexible joint parallel manipulators, M.S. Thesis, 2006, Middle East Technical University, Ankara, Turkey.

[19] S.K. Ider, F.M.L. Amirouche, Numerical stability of the constraints near singular positions in the dynamics of multibody systems, *Computers and Structures* 33 (1989) 129–137.

[20] Kollmorgen Inland Motor, Handbook for Brushless Motors and Drive Systems, VA, 1996.